Pion emission from the T2K replica target: method, results and application

N. Abgrall[1a], A. Aduszkiewicz[b], T. Anticic[c], N. Antoniou[d], J. Argyriades[a], B. Baatar[e], A. Blondel[a], J. Blumer[f], M. Bogomilov[x], A. Bravar[a], W. Brooks[i], J. Brzychczyk[j], A. Bubak[k], S. A. Bunyatov[e], O. Busygina[l], P. Christakoglou[d], P. Chung[n], T. Czopowicz[g], N. Davis[d], S. Debieux[a], S. Di Luise[o], W. Dominik[b], J. Dumarchez[p], K. Dynowski[g], R. Engel[f], A. Ereditato[q], L. S. Esposito[o], G. A. Feofilov[r], Z. Fodor[h], A. Ferrero[a], A. Fulop[h], M. Gaździcki[s], M. Golubeva[l], B. Grabez[aa], K. Grebieszkow[g], A. Grzeszczuk[k], F. Guber[l], A. Haesler[a], H. Hakobyan[i], T. Hasegawa[v], R. Idczak[w], S. Igolkin[r], Y. Ivanov[i], A. Ivashkin[l], K. Kadija[c], A. Kapoyannis[d], N. Katryńska[w], D. Kiełczewska[b], D. Kikola[g], M. Kirejczyk[b], J. Kisiel[k], T. Kiss[h], S. Kleinfelder[ab], T. Kobayashi[v], O. Kochebina[r], V. I. Kolesnikov[e], D. Kolev[x], V. P. Kondratiev[r], A. Korzenev[a], S. Kowalski[k], A. Krasnoperov[e], S. Kuleshov[i], A. Kurepin[l], R. Lacey[n], D. Larsen[z], A. Laszlo[h], V. V. Lyubushkin[e], M. Maćkowiak-Pawłowska[g], Z. Majka[j], B. Maksiak[g], A. I. Malakhov[e], D. Maletic[aa], A. Marchionni[o], A. Marcinek[j], I. Maris[f], V. Marin[l], K. Marton[h], T. Matulewicz[b], V. Matveev[l,e], G. L. Melkumov[e], M. Messina[q], St. Mrówczyński[s], S. Murphy[a], T. Nakadaira[v], K. Nishikawa[v], T. Palczewski[y], G. Palla[h], A. D. Panagiotou[d], T. Paul[f], W. Peryt[g], O. Petukhov[l], R. Płaneta[j], J. Pluta[g], B. A. Popov[e,p], M. Posiadała[b], S. Puławski[k], J. Puzovic[aa], W. Rauch[u], M. Ravonel[a], R. Renfordt[t], A. Robert[p], D. Röhrich[z], E. Rondio[y], B. Rossi[q], M. Roth[f], A. Rubbia[o], A. Rustamov[t], M. Rybczyński[s], A. Sadovsky[l], K. Sakashita[v], M. Savic[aa], T. Sekiguchi[v], P. Seyboth[s], M. Shibata[v], R. Sipos[h], E. Skrzypczak[b], M. Słodkowski[g], P. Staszel[j], G. Stefanek[s], J. Stepaniak[y], C. Strabel[o], H. Ströbele[t], T. Susa[c], M. Szuba[f], M. Tada[v], A. Taranenko[n], V. Tereshchenko[e], T. Tolyhi[h], R. Tsenov[x], L. Turko[w], R. Ulrich[f], M. Unger[f], M. Vassiliou[d], D. Veberič[f], V. V. Vechernin[r], G. Vesztergombi[h], A. Wilczek[k], Z. Włodarczyk[s], A. Wojtaszek-Szwarc[s], O. Wyszyński[j], L. Zambelli[p], W. Zipper[k],

The NA61/SHINE Collaboration,

[1]Corresponding author, nicolas.abgrall@cern.ch

V. Galymov[ac], M. Hartz[ac,ad], A. K. Ichikawa[ae], H. Kubo[ae], A. D. Marino[af], K. Matsuoka[ae], A. Murakami[ae], T. Nakaya[ae], K. Suzuki[ae], T. Yuan[af], E. D. Zimmerman[af]

[a] *University of Geneva, Geneva, Switzerland*
[b] *Faculty of Physics, University of Warsaw, Warsaw, Poland*
[c] *Rudjer Boskovic Institute, Zagreb, Croatia*
[d] *University of Athens, Athens, Greece*
[e] *Joint Institute for Nuclear Research, Dubna, Russia*
[f] *Karlsruhe Institute of Technology, Karlsruhe, Germany*
[g] *Warsaw University of Technology, Warsaw, Poland*
[h] *Wigner Research Centre for Physics, Budapest, Hungary*
[i] *Universidad Tecnica Federico Santa Maria, Valparaiso, Chile*
[j] *Jagiellonian University, Cracow, Poland*
[k] *University of Silesia, Katowice, Poland*
[l] *Institute for Nuclear Research, Moscow, Russia*
[m] *Pusan National University, Pusan, Republic of Korea*
[n] *State University of New York, Stony Brook, USA*
[o] *ETH, Zurich, Switzerland*
[p] *LPNHE, University of Paris VI and VII, Paris, France*
[q] *University of Bern, Bern, Switzerland*
[r] *St. Petersburg State University, St. Petersburg, Russia*
[s] *Jan Kochanowski University in Kielce, Poland*
[t] *University of Frankfurt, Frankfurt, Germany*
[u] *Fachhochschule Frankfurt, Frankfurt, Germany*
[v] *High Energy Accelerator Research Organization (KEK), Tsukuba, Ibaraki-ken, Japan*
[w] *University of Wrocław, Wrocław, Poland*
[x] *Faculty of Physics, University of Sofia, Sofia, Bulgaria*
[y] *National Centre for Nuclear Research, Warsaw, Poland*
[z] *University of Bergen, Bergen, Norway*
[aa] *University of Belgrade, Belgrade, Serbia*
[ab] *University of California, Irvine, USA*
[ac] *York University, Toronto, Canada*
[ad] *University of Toronto, Toronto, Canada*
[ae] *Kyoto University, Kyoto, Japan*
[af] *University of Colorado, Boulder, USA*

Abstract

The T2K long-baseline neutrino oscillation experiment in Japan needs precise predictions of the initial neutrino flux. The highest precision can be reached based on detailed measurements of hadron emission from the same target as

used by T2K exposed to a proton beam of the same kinetic energy of 30 GeV. The corresponding data were recorded in 2007–2010 by the NA61/SHINE experiment at the CERN SPS using a replica of the T2K graphite target. In this paper details of the experiment, data taking, data analysis method and results from the 2007 pilot run are presented. Furthermore, the application of the NA61/SHINE measurements to the predictions of the T2K initial neutrino flux is described and discussed.

Keywords: hadron production, long target, neutrino flux predictions

1. Introduction

Neutrino beams have become a major tool to perform studies of neutrino properties. At the T2K long-baseline neutrino oscillation experiment in Japan [1, 2], a high-intensity neutrino beam is produced at J-PARC by a 30 GeV proton beam impinging on a 90 cm long graphite target. A schematic view of the neutrino beamline is shown in Fig. 1. Positively charged hadrons exiting the target (mainly π and K mesons) are focused by a set of three magnetic horns and decay along a 96 m long decay tunnel. The flavour content and energy spectrum of the beam are measured at the near detector complex located 280 m away from the target station, and by the Super-Kamiokande (SK) detector at a distance of 295 km. For the first time in the history of accelerator-based neutrino experiments, T2K adopted the off-axis technique [3] to generate a dedicated neutrino beam with the off-axis angle set to 2.5° for both the near and far detectors.

T2K was the first experiment to make a direct measurement of a non-zero value of the θ_{13} mixing angle via $\nu_\mu \to \nu_e$ appearance. The published 90 % CL inclusion interval of $0.03(0.04) < \sin^2 2\theta_{13} < 0.28(0.34)$ for the normal (inverted) mass hierarchy, $\delta_{CP} = 0$, $\sin^2 2\theta_{32} = 1$ and $\Delta m^2_{32} = 2.4 \times 10^{-3}$ eV^2 was obtained with only 2 % of the final statistics [4]. Later, these results were confirmed with greater precision by measurements of electron anti-neutrino disappearance at reactors [5, 6]. With the same set of data T2K also provided new measurements of the neutrino oscillation parameters $\sin^2 2\theta_{32}$ and Δm^2_{32} by studying ν_μ disappearance [7], and aims at a precision of 1 % for $\sin^2 2\theta_{32}$ and 3 % for Δm^2_{32} for the full statistics.

Although neutrino beams provide well defined and controlled sources of neutrinos, intrinsic uncertainties on the fluxes predicted with Monte Carlo (MC) simulations arise from models employed to simulate hadron emission

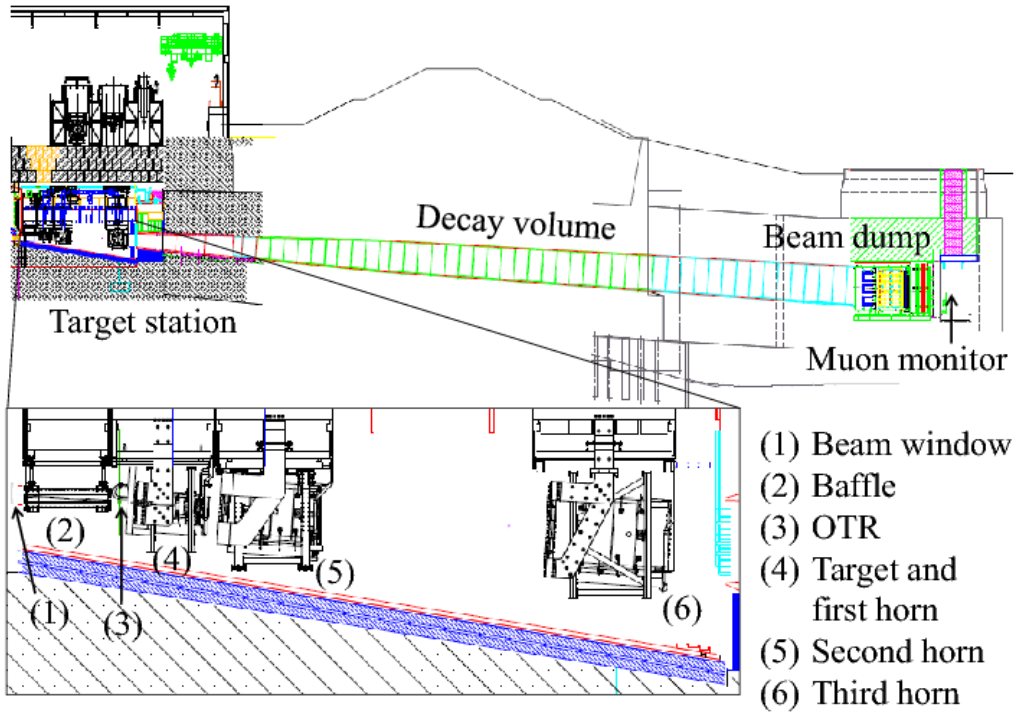

Figure 1: A side view of the T2K neutrino beamline. See Ref. [2] for a detailed description and for notations used.

from long nuclear targets used in accelerator based experiments. In these types of experiments, a non-negligible fraction of the neutrino flux actually arises from particles which are produced in hadronic re-interactions in the long target. Up to now, neutrino flux predictions have been (if ever) constrained by using either parametrizations based on existing hadron production data available in literature, e.g. [8, 9, 10], or dedicated hadron production measurements performed on thin nuclear targets, e.g. HARP p+Al data [11] for K2K [12], HARP p+Be data [13] for MiniBooNE [14] and SciBooNE, SPY p+Be data [15] for NOMAD [16]. T2K recently followed this approach by using the NA61/SHINE results on p+C interactions at 30 GeV extracted from measurements of hadron production in a thin (2 cm) graphite target [17, 18].

Although such measurements provide constraints on the production of

secondary particles in the primary interaction of the beam protons in the target, the lack of direct measurements of the production of tertiary particles in re-interactions, and hence the use of sparse data sets to cover these contributions, limits the achievable precision of the flux prediction. The main motivation for measurements of hadron emission from a replica of the T2K target is therefore to reduce the systematic uncertainties on the prediction of the initial neutrino flux originating from products of interactions in the target.

The NA61/SHINE (SPS Heavy Ion and Neutrino Experiment) experiment at the CERN Super Proton Synchrotron (SPS) is pursuing a rich physics program in various fields [19, 20, 21, 22] from precise hadron production measurements for T2K and more reliable simulations of cosmic-ray air showers for the Pierre Auger and KASCADE experiments [23, 24], to the study of the properties of the onset of deconfinement with measurements of p+p, p+Pb and nucleus+nucleus collisions at the SPS energies.

In addition to recently published thin-target (0.04 λ_I) measurements of charged pion and kaon production [17, 18] already used for the T2K neutrino flux predictions [4, 7], the NA61/SHINE collaboration studies hadron emission from a replica of the T2K target (1.9 λ_I) exposed to a 30 GeV proton beam. A total of 0.2×10^6 events were recorded during a pilot data taking in 2007. High statistics data were recorded in 2009 (4×10^6 events) and 2010 (10×10^6 events). For the first time, the kinematical phase space of pions and kaons exiting the target and producing neutrinos in the direction of the near and far detectors is fully covered by a single hadron production experiment.

The long-target analysis presented in this paper uses the low-statistics data collected in 2007. It however sets the ground for the ongoing analysis of high-statistics NA61/SHINE data with the replica of the T2K target. It demonstrates that high-quality long-target data were successfully taken with the NA61/SHINE apparatus for T2K, and that such data can be used effectively to constrain the T2K neutrino flux predictions. A comparison of neutrino flux predictions based on thin-target hadron production measurements and long-target hadron emission measurements is performed as an illustration of the complete procedure.

This paper is organised as follows: Section 2 briefly reviews the current T2K flux predictions based on the NA61/SHINE thin-target data and points out the need for additional long-target measurements to improve the precision of the predictions. Section 3 describes the NA61/SHINE experimental setup, kinematical coverage of the data, event selection and data normalisa-

tion, reconstruction method and particle identification. The NA61/SHINE simulation chain is presented in Section 4. Yields of positively charged pions measured at the surface of the replica of the T2K target are given in Section 5. Possible strategies to use long-target measurements in the T2K beam simulation are proposed in Section 6 which also provides an illustration of the complete procedure.

2. Requirements on hadron production data for the prediction of T2K neutrino fluxes

The T2K beam MC simulation [2] is used to predict the initial neutrino flux at the near and far detectors. It comprises a full description of the beam line, including the target, magnetic horns, decay tunnel and beam dump. Hadronic interactions in the target are simulated by the FLUKA2008.3b [25] model. The propagation of outgoing particles is then modeled by the GEANT3 [26] package with GCALOR [27] for hadronic interactions.

Measurements of particle emission from the replica of the T2K target are necessary to constrain the model calculations and to reach a 5 % precision on the absolute flux prediction as required by the T2K physics goals (i.e. 3 % precision on the ratio of the far to near fluxes for precision ν_μ disappearance and ν_e appearance analyses).

Predictions obtained for horn currents of 250 kA are shown in Fig. 2 for the ν_μ and ν_e fluxes at the near detector. The ν_μ flux below 2 GeV predominantly (95 %) originates from the in-flight decay of positively charged pions focused by the magnetic horns of the beam line (see Ref. [2] for a detailed description of the T2K beam line). The ν_e flux is dominantly produced by the decay of positively charged kaons above 1.5 GeV, whereas at lower energy ν_e's originate mostly from the decay of pions via the subsequent muon decay, i.e. $\pi^+ \to \mu^+\nu_\mu$ followed by $\mu^+ \to e^+\nu_e\bar{\nu}_\mu$. Thus, pion production data can constrain most of the ν_μ flux and a significant fraction of the ν_e flux below 2 GeV neutrino energy.

In terms of hadron production measurements, neutrino fluxes can be decomposed into *secondary* and *tertiary* components. The *secondary* component originates from neutrino parents produced in the primary interaction of the beam protons in the target, e.g. secondary pions, $p + C \to \pi^+ + X$. This *secondary* component can be constrained mainly by pion (and kaon) production cross-sections obtained from measurements on a thin target. The

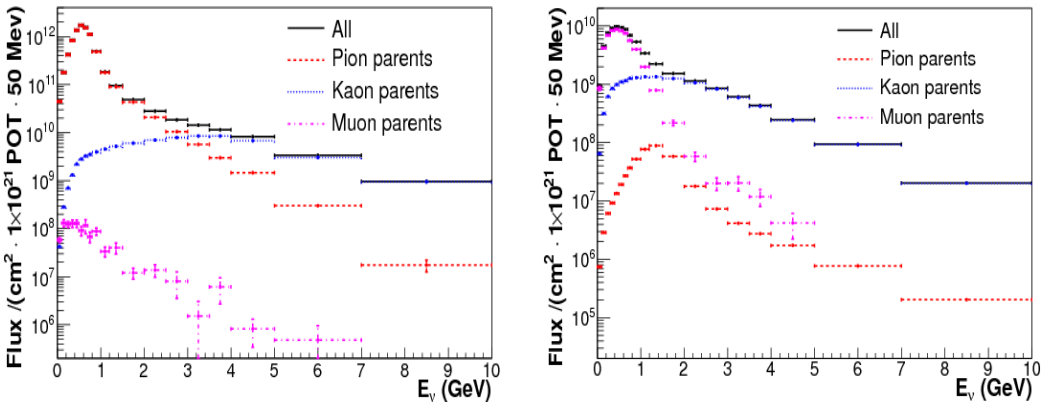

Figure 2: Prediction (based on FLUKA2008.3b and re-weighted by the NA61 thin target data) of the ν_μ [left] and ν_e [right] fluxes at the near detector of T2K. The contribution of different parent particles to the total flux are shown.

tertiary component refers to neutrino parents produced in interactions of secondary particles, whether such interactions occur in the target or out of the target in the elements of the beamline. The contribution to the neutrino flux from parents produced in the target is therefore defined as the sum of the *secondary* component and the *tertiary* component due to interactions in the target. This contribution can be obtained from measurements of pion (and kaon) emission from a replica target.

The dependence of the *secondary* and *tertiary* contributions on the neutrino energy is depicted in Fig. 3 for the ν_μ and ν_e fluxes at the far detector. The *secondary* component contributes 60 % of the ν_μ (ν_e) flux at the peak of the beam energy spectrum (600 MeV). The remaining 40 % constitutes the *tertiary* component due to interactions in the target and elements of the beam line. Thus, thin-target measurements for T2K (i.e. positively charged pion and kaon inclusive production cross-sections at 30 GeV [17, 18]) can directly constrain up to 60 % of the ν_μ (ν_e) flux prediction.

The lack of direct measurements of secondary interactions however requires in most cases scaling to energies and nuclei relevant for the T2K experimental setup, as well as extrapolating to uncovered regions of the kinematical phase space. Such procedures have been used in addition for the T2K flux prediction. This brings in new sources of systematic uncertainties on top of the uncertainty of the measurements.

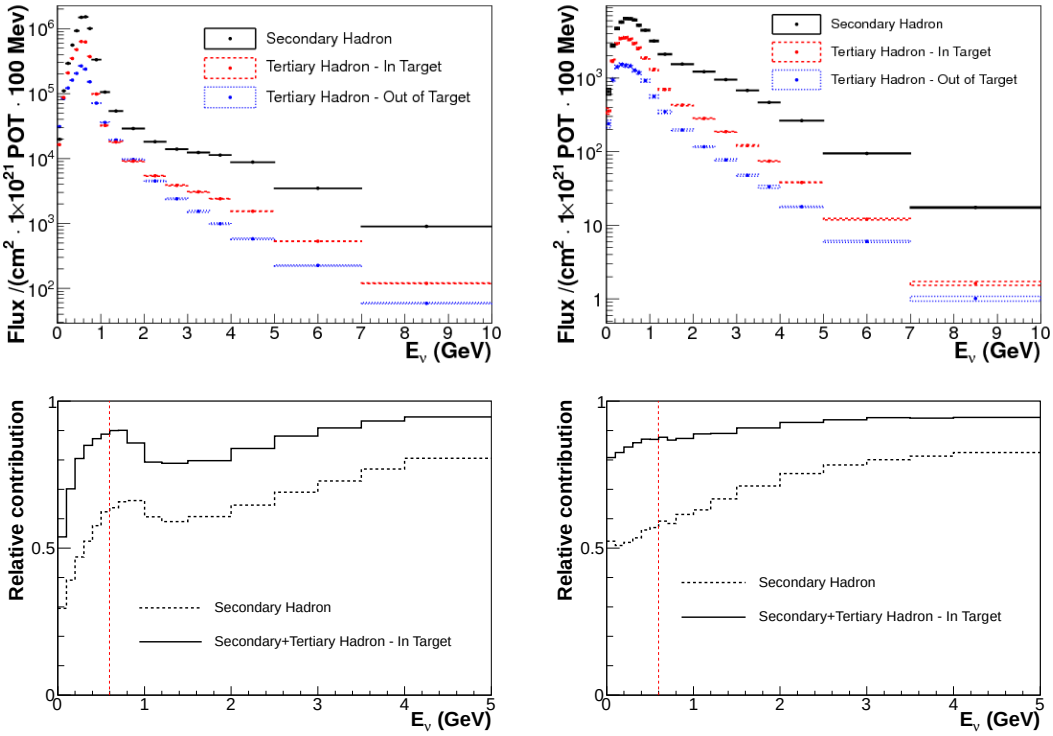

Figure 3: *Secondary* and *tertiary* components of the ν_μ [top left] and ν_e [top right] fluxes at the far detector. The contribution of parents originating from the target sums up to 90 %, among which 60 % are due to the *secondary* component and 30 % due to re-interactions in the target (the in-target component). The relative contributions of the secondary and total in-target (secondary+tertiary in-target) components are shown for ν_μ [bottom left] and ν_e [bottom right] as a function of energy. The dashed vertical line shows the location of the peak of the beam energy spectrum (600 MeV). Predictions are based on FLUKA2008.3b and re-weighted by the NA61 thin-target data.

As an example, the systematic errors of the ν_μ and ν_e flux predictions at the far detector for the first published T2K analysis are depicted in Fig. 4. Details about the procedure developed to re-weight the original predictions of the T2K beam simulation (based on FLUKA2008.3b) with the NA61 thin-target data are given elsewhere [28]. The total fractional error on the ν_μ and ν_e fluxes is about 15 % at the peak of the beam energy spectrum. At this energy the fractional error attributed to the re-weighting of tertiary pions produced in interactions of secondary nucleons is about half the size of that associated with the re-weighting of secondary pions. However the error

associated with the production of the related secondary nucleons is of the same order. The achievable precision on the flux prediction based on thin-target data alone is therefore limited due to the uncertainty on the *tertiary* component of the flux.

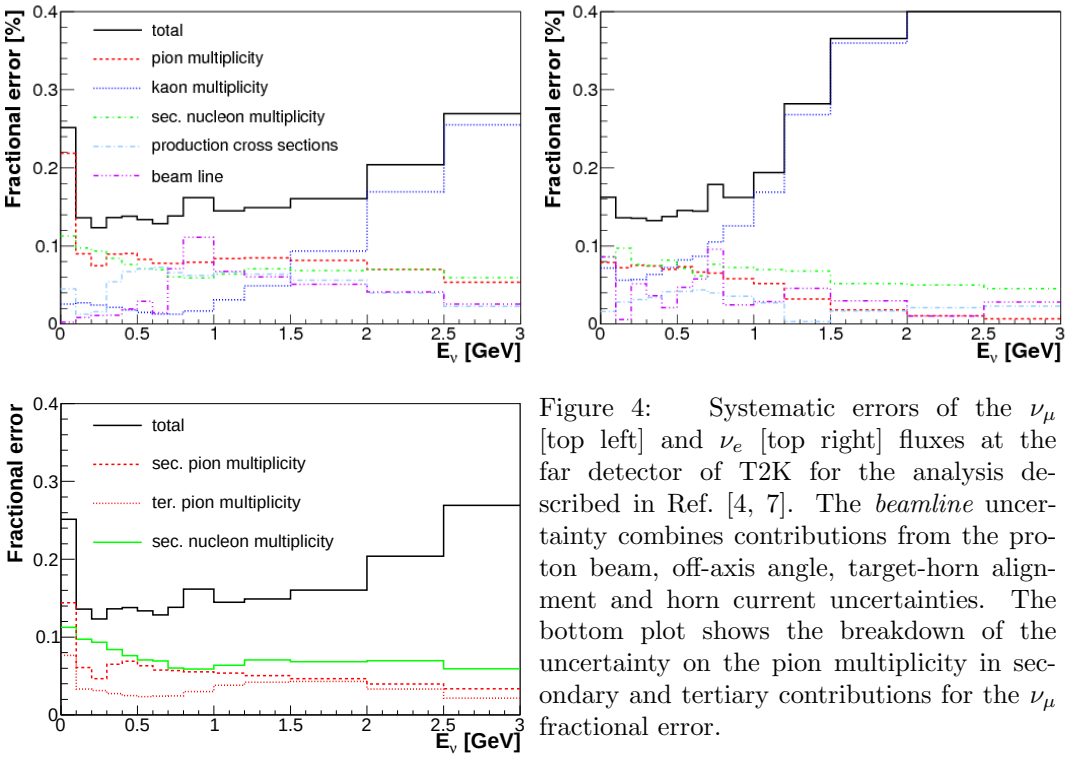

Figure 4: Systematic errors of the ν_μ [top left] and ν_e [top right] fluxes at the far detector of T2K for the analysis described in Ref. [4, 7]. The *beamline* uncertainty combines contributions from the proton beam, off-axis angle, target-horn alignment and horn current uncertainties. The bottom plot shows the breakdown of the uncertainty on the pion multiplicity in secondary and tertiary contributions for the ν_μ fractional error.

Measurements of particle emission from a full-size replica of the T2K target have the advantage to cover at once the production of secondary particles exiting the target, as well as the emission of particles originating from secondary interactions inside the target. Such measurements can be used in a single-step approach in which simulated yields of outgoing particles are directly re-weighted by yields measured at the surface of the target. In this case, uncertainties on the flux predictions are almost entirely limited to the uncertainties of the measurements. Actually, as depicted in Fig. 3, at the peak of the beam energy spectrum the *secondary* component and the *tertiary* component due to interactions in the target sum up to 90 % of the ν_μ (ν_e) flux. Hadron emission measurements with the replica of the T2K target (i.e. yields of charged pions and kaons exiting the target) can thus constrain up

to 90 % of the flux prediction.

Note that both thin-target and replica-target based approaches are necessary as discrepancies observed in a comparison of a flux prediction based on thin-target data to one obtained when yields of outgoing particles are re-weighted with the replica-target data would point to an inappropriate re-weighting of the secondary interactions in the target. Such comparisons would allow further precise tuning of the employed hadron production model.

3. The NA61/SHINE replica-target measurements for T2K

3.1. Experimental setup

The NA61 detector is a large acceptance spectrometer located in the North Area H2 beam line of the CERN SPS. Most detector components were inherited from the NA49 experiment and are described in detail in Ref. [29]. The detector consists of a set of five time projection chambers (TPCs). Two of them, called Vertex TPCs (VTPC-1 and VTPC-2), are placed inside superconducting dipole magnets. The magnetic field was set to 1.14 Tm in order to optimize the geometrical acceptance for the T2K measurements. A small TPC is placed between VTPC-1 and VTPC-2 and is referred to as the GAP TPC. Two large TPCs, the Main TPCs (MTPC-L and MTPC-R), are positioned downstream of the VTPC-2, symmetrically with respect to the beamline. The set of TPCs is complemented by time-of-flight (ToF) detectors located downstream of the MTPCs. Before the 2007 run the experiment was upgraded with a new forward time-of-flight detector (ToF-F) in order to extend the acceptance. The ToF-F consists of 64 scintillator bars with photomultiplier (PMT) readout at both ends resulting in a time resolution of about 115 ps. An overview of the NA61 setup is shown in Fig. 5 together with the definition of the NA61 coordinate system.

The replica of the T2K target used in NA61 consists of a 90 cm (1.9 λ_I) long graphite rod of density $\rho = 1.83$ g/cm^3. The downstream face of the target was located 52 cm upstream of the mylar entrance window of VTPC-1, and the target was held in position by aluminium support flanges fixed at its upstream end. The replica and the actual target of T2K in its complete environment are shown in the drawings in Fig. 6. There are small differences between the two targets. Systematic uncertainties related to these differences have been studied and are reported in Sec. 6.2.

A 15 kHz beam rate was used during the 2007 measurements. Due to the thickness of the replica target each beam proton is assumed to interact in the

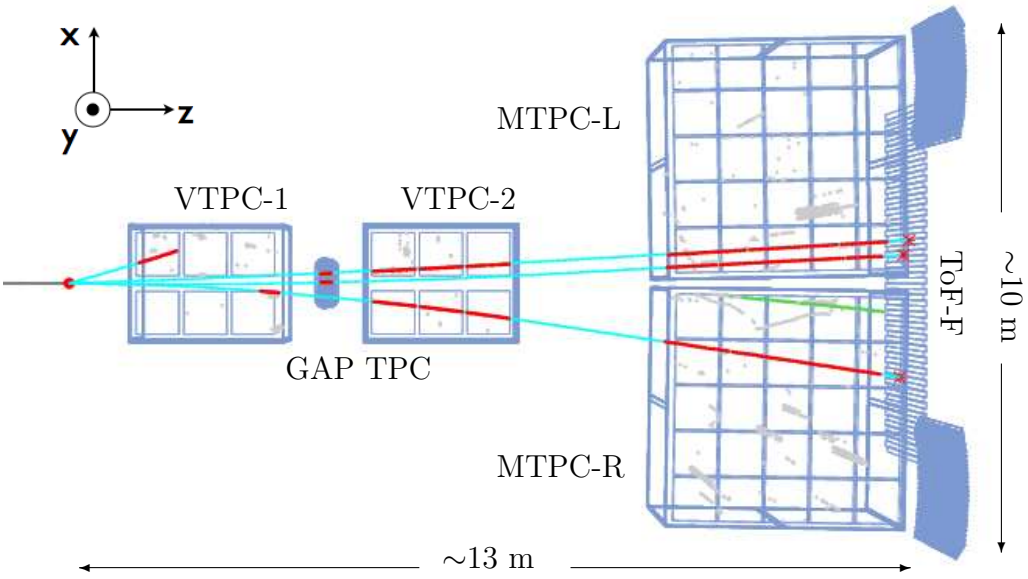

Figure 5: An example of a reconstructed p+C interaction at 30 GeV beam energy in the replica of the T2K target showing tracks reconstructed in the TPCs and associated with hits in the ToF-F detector. The incoming beam direction is along the z axis. The magnetic field bends the trajectory of outgoing charged particles in the $x-z$ (horizontal) plane. The drift direction in the TPCs is along the y axis.

target and the trigger simply consists of selecting all beam protons by using a coincidence of various counters and vetos along the beam line (see [17] for more details). In particular, the so-called S1 scintillation counter provides timing information and triggers the data acquisition from the TPCs and ToF detectors. The 100 ns dead time of S1 results in a 0.2 % pile up probability. The trajectory of each beam proton is reconstructed in a telescope of three beam position detectors that allows the determination of the position of the beam at the upstream face of the target with a precision of better than 300 μm in both directions.

More details on the experimental setup, detector calibration and performance as well as a description of the proton identification in the beam are given elsewhere [17].

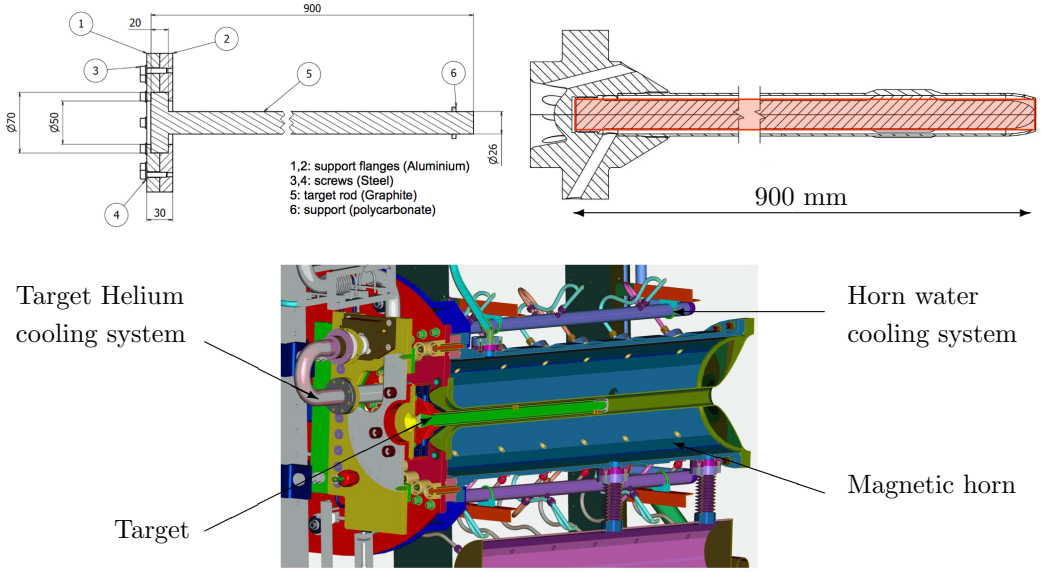

Figure 6: Technical drawing with dimensions given in mm (side view) of the replica target used during the NA61 data taking [top left] consisting of a 90 cm long graphite rod and aluminium support flanges. Drawing of the complete geometry of the T2K target [top right]. The overlaid red rectangle represents the simplified geometry of the replica target. View of the T2K target and its cooling envelope embedded in the first focusing horn of the T2K beamline [bottom].

3.2. Coverage of the T2K kinematical phase space in NA61/SHINE

The phase space of interest for positively charged pions that exit the T2K target and produce neutrinos in the direction of the far detector is depicted in Fig. 7 as a function of (p, θ), where p is the laboratory momentum of the pion at the surface of the target, and θ is the angle of its direction calculated with respect to the beam axis. For comparison the binning used in the NA61 data analysis is overlaid.

The phase space of interest is divided into two kinematical regions: pions which exit from the side of the target with emission peaking at large angle and low momentum, and pions exiting from the downstream face which populate mainly the region of small angle and large momenta. In the T2K beam line the latter are not(or less) focused by the magnetic horns and are mainly the pions that decay to muons with momentum larger than 5 GeV/c. These muons are detected by the muon monitor (MUMON) located downstream of the beam dump and provide a spill-by-spill monitoring of the direction of the

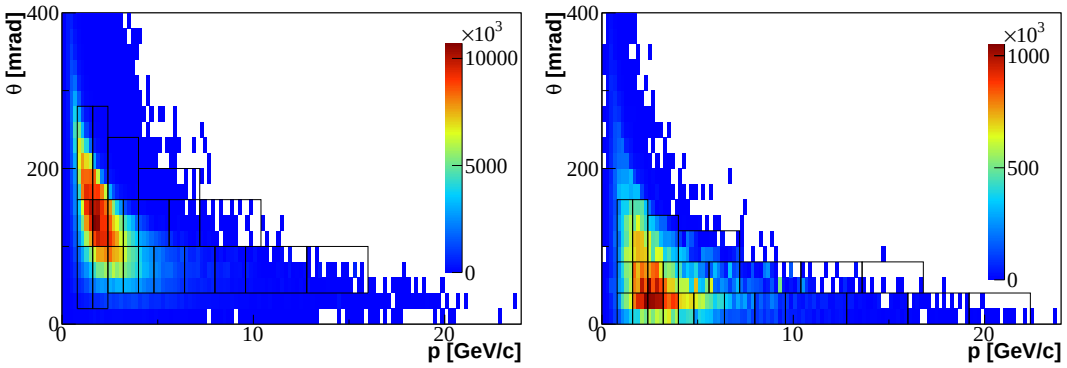

Figure 7: Kinematical phase space of positively charged pions (for 10^{21} pot) exiting from the side of the target (summed over five longitudinal bins along the target, see text) [left] or from the downstream face [right], and producing neutrinos in the direction of the far detector of T2K. The respective analysis binning of the NA61 data with the replica of the T2K target is overlaid on top. Predictions obtained from the T2K beam simulation.

beam [2, 30]. The comparison of the MUMON measurements to the beam simulation is thus an important step in the validation of the MC model. For that purpose, in NA61 a dedicated run was taken in 2010 with a replica of the T2K target to measure precisely the very forward region of particle production below 20 mrad polar angle. In this run, the spectrometer was operated with the highest magnetic field configuration (of about 9 Tm), which deflected forward going particles into the sensitive regions of the TPCs, thus avoiding the uninstrumented region along the beam axis.

The binning for the analysis in (p, θ) is driven by the acceptance of the NA61 apparatus. As shown in Fig. 7, it covers most of the region of interest for T2K. The relatively large size of the bins, ranging from 0.8 to 3.2 GeV/c in momentum and from 40 to 120 mrad in polar angle, is due to the low statistics of the 2007 data. In addition to (p, θ), data are further binned with respect to the longitudinal position of the outgoing particles at the surface of the target. As shown in Fig. 6, part of the T2K target is embedded in the first magnetic horn of the beam line. In this configuration and due to the extension of the target, the focusing properties of the horn depend on the longitudinal position of the outgoing particles. We investigated this effect with the T2K beam MC and determined that at least five longitudinal bins are required to obtain a prediction that does not differ significantly from a nominal non-binned prediction in terms of mean neutrino energy and overall

normalisation. Five bins of 18 cm each are therefore used along the beam direction. An additional bin is used for the downstream face of the target.

The acceptance of the NA61 detector in (p, θ) does not vary by more than 10 % over the length of the target for pions exiting the side of the target. An identical (p, θ) binning is therefore applied to all longitudinal bins along the target. For pions exiting the downstream face of the target, the coverage extends to higher momenta. The same binning in p is maintained while a finer binning is used for the polar angle θ. The azimuthal acceptance of the detector in the $x - y$ plane is however highly non-uniform due to the finite extent of the TPCs along the drift direction (y axis) and the uninstrumented region of the detector along the beam line. This is illustrated in Fig. 8 which depicts the distribution of azimuthal angle ϕ of the TPC tracks (in the flat regions the track reconstruction efficiency is very close to 100%). For this reason, the NA61 replica-target data cannot be used as a direct input on a track-by-track basis in the T2K beam simulation for the flux predictions. Other suitable methods are therefore considered in Section 6.1.

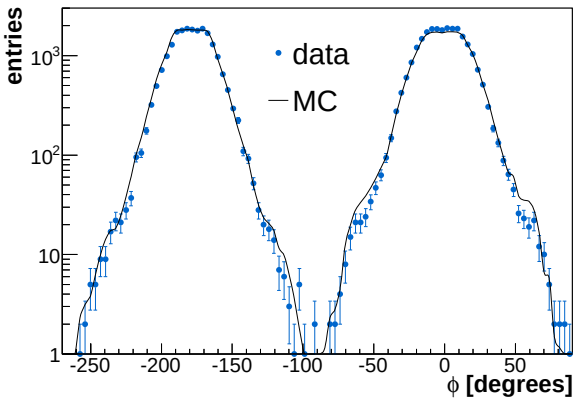

Figure 8: Distribution of the azimuthal angle, ϕ, of all TPC tracks in data (markers) and MC (line).

3.3. Event selection and data normalisation

As mentioned in Section 3.1, the NA61 beam is defined by a set of scintillation and veto counters along the beam line and the proton beam tracks are reconstructed in three beam position detectors. The beam tracks are further selected to assure that protons hit the upstream face of the target. The selection is based on two main cuts: the first one on the χ^2 of the fit of the beam tracks, the second on the extrapolated position on the upstream face of the target. The selection rejects 32 % of the events.

The distribution of beam particles in time with respect to the trigger time is shown in Fig. 9 over a 40 μs time window. Due to the relatively high beam intensity, about 40 % of the events include a second beam particle within $\pm$25 μs around the trigger time. The acquisition window of the TPCs extends over a maximum drift time of 50 μs for the gas composition and drift voltages applied in 2007. Multiple interactions can therefore occur in the target during a single acquisition window. Such interactions result in so-called *off-time* tracks, i.e. tracks reconstructed in the TPCs but not associated in time with the beam proton that triggered the acquisition system.

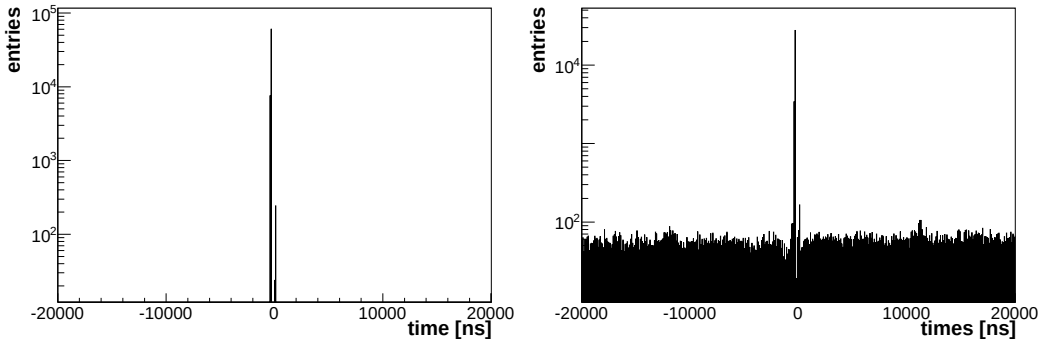

Figure 9: Time distribution of beam particles in a 40 μs time window for single beam particle events [left] ($\sim$60 % of all events), and events with two beam particles [right] ($\sim$40 % of all events). The beam time is centered at -300 ns.

Since the measured yields are normalized to the number of protons on target, tracks reconstructed in the TPCs are associated to the triggering beam proton by requiring a signal in the appropriate ToF-F detector.

Actually, for the 2007 beam rate, tracks that leave a valid signal in the ToF-F can only have been produced in the interaction of the same beam proton in the target since the 100 ns acquisition window of the detector is much smaller than the mean distance in time between two beam particles. Hits associated with off-time tracks in the ToF-F detector result in overflows which are rejected at the analysis level. The effect of this cut on the track multiplicity in the TPCs is depicted in Fig. 10. Although many beam particles are present in a $\pm$25 μs window around the beam time, the track multiplicity in the TPCs is consistent with that of single-interaction events once the ToF-F requirement is applied.

The NA61 yields from the replica of the T2K target are thus normalised to

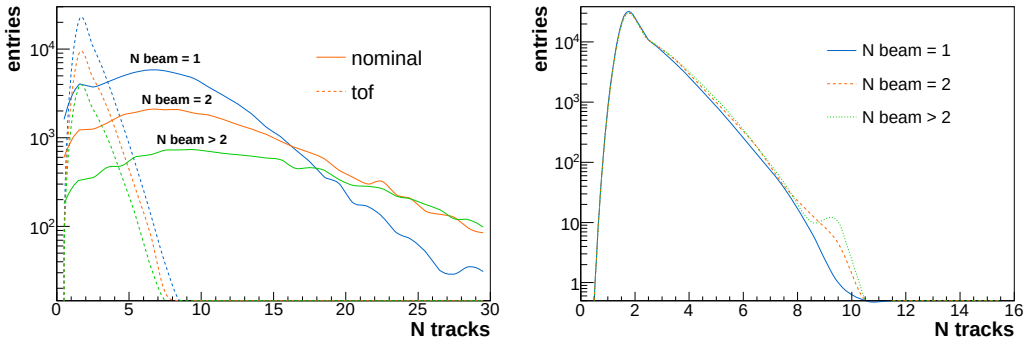

Figure 10: Track multiplicity in the TPCs without (solid) and with (dashed) the ToF-F requirement for events with different numbers of beam particles [left]. Multiplicity distributions normalised to the number of single beam particle events with the ToF-F requirement [right].

the total number of protons on target which produced a valid trigger. After the quality cuts described above, a total of 114 885 events were selected for this analysis.

3.4. Reconstruction of track parameters at the surface of the target

Reconstruction algorithms applied for the analysis described here are based on those used to produce the NA61 thin-target results with the exception that the fitting procedure at the primary interaction vertex is replaced by a backward extrapolation procedure to the surface of the replica target. The main steps of the reconstruction are:

(i) cluster finding in the TPC raw data and calculation of the cluster weighted mean position and total charge,

(ii) reconstruction of local track segments in each TPC separately,

(iii) matching of track segments from different TPCs into global tracks,

(iv) track fitting through the magnetic field and determination of the track parameters at the first measured TPC cluster,

(v) matching of ToF-F hits with TPC tracks,

(vi) backward extrapolation of the global tracks from their first measured TPC cluster to the surface of the target.

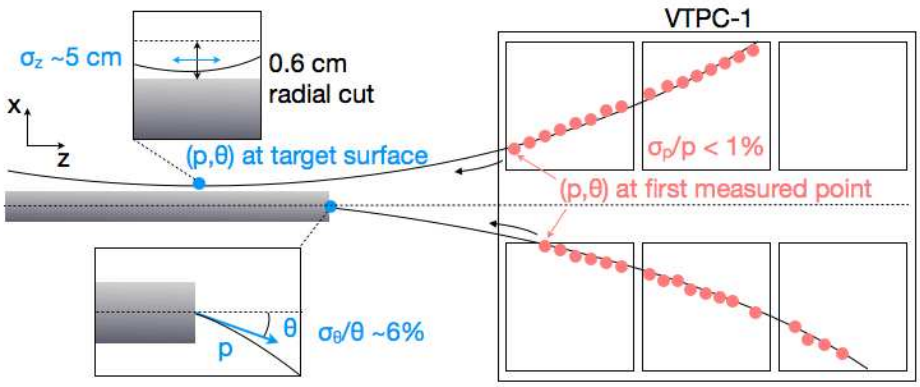

Figure 11: Sketch depicting the backward extrapolation of TPC tracks onto the surface of the target. The point of closest approach is determined and the track parameters p and θ are calculated at this point. Only tracks for which this point lies within a distance of 0.6 cm around the target surface are accepted. The resolution for the different track parameters are also given in the figure.

The backward extrapolation procedure is depicted in Fig. 11. If the extrapolated trajectory crosses the surface of the target at a certain position, the track parameters and associated covariance matrix are determined at this point. Otherwise a minimisation procedure is performed along the length of the target to find a point of closest approach between the track trajectory and the surface of the target. The track parameters are then determined at this point. Tracks are associated with the target if the point of closest approach is found within 0.6 cm from the surface of the target. This value actually corresponds to the mean radial uncertainty of the extrapolation over the full length of the target.

The resolution of the track parameters, p and θ, at the surface of the target is driven by that estimated at the first fitted TPC cluster. The latter strongly depends on the track topology. In order to improve the resolution, tracks are therefore grouped into four topologies and specific cuts on the minimum number of clusters on track are applied to each class. For all tracks a minimum number of 40 clusters is required in the MTPCs as well as a valid signal in the ToF-F detector. The following topologies are defined: the VTPC-1+VTPC-2 topology corresponds to tracks with segments in both VTPCs, while the VTPC-1 and VTPC-2 topologies correspond to tracks with a segment in one VTPC only. The GAP TPC topology corresponds to tracks

which have measured points only in the small GAP TPC and a MTPC. Examples of such topologies (VTPC-2, GAP TPC and VTPC-1+VTPC-2 from top to bottom) are shown in Fig. 5. A minimum of 40 clusters in the VTPC-1 is required for the VTPC-1 topology, 45 clusters for the VTPC-2 topology, 50 clusters for the VTPC-1+VTPC-2 topology and 6 clusters for the GAP TPC topology. In addition, tracks are required to be reconstructed in a ± 30 degree symmetrical wedge in the azimuthal angle with respect to the x-axis. The quality cuts mentioned above are used to define the detector acceptance for all related MC studies in what follows.

After a calibration procedure described in details in Ref. [17], the spatial resolution on TPC measurements (including the relative alignment between different TPCs) is better than 0.5 mm.

The resolution of p and θ at the first TPC cluster are shown in Fig. 12 as a function of momentum for the different toplogies. In particular, the GAP TPC tracks have their momentum measured with a maximum of 7 clusters in the magnetic field in the very forward region of the spectrometer. Hence the larger error on the polar angle and a worse momentum resolution. The resolution obtained after the backward extrapolation to the surface of the target is estimated to be $\sigma_\theta/\theta = 6\%$ for the polar angle. The resolution on the longitudinal position depends on the track topology and its average value for the analyzed track sample is $\sigma_z = 5$ cm.

A precise knowledge of the relative alignment of the target and the beam is needed to reconstruct tracks at the surface of the target in bins of (p, θ, z). The position of the long target was first measured by surveyors. In addition, a procedure based on the backward extrapolation of the TPC tracks was developed to refine the measured position of the target with respect to the beam axis. For that purpose, the position of the upstream face of the target is used as a reference. It is actually precisely determined by the independent extrapolations of the TPC tracks from the downstream region, and that of the beam tracks from the upstream region.

Once the target position is known, the beam profile and radial distribution on the upstream face are determined by extrapolating the beam tracks reconstructed in the beam position detectors. These distributions for the 2007 run are shown in Fig. 13 together with the positions of the upstream and downstream faces of the target.

In 2007, the target was shifted upwards by 0.4 cm and tilted in the horizontal (vertical) plane by 5 (2.8) mrad. The hardware target alignment technique was improved before the 2009 data-taking period. For this data

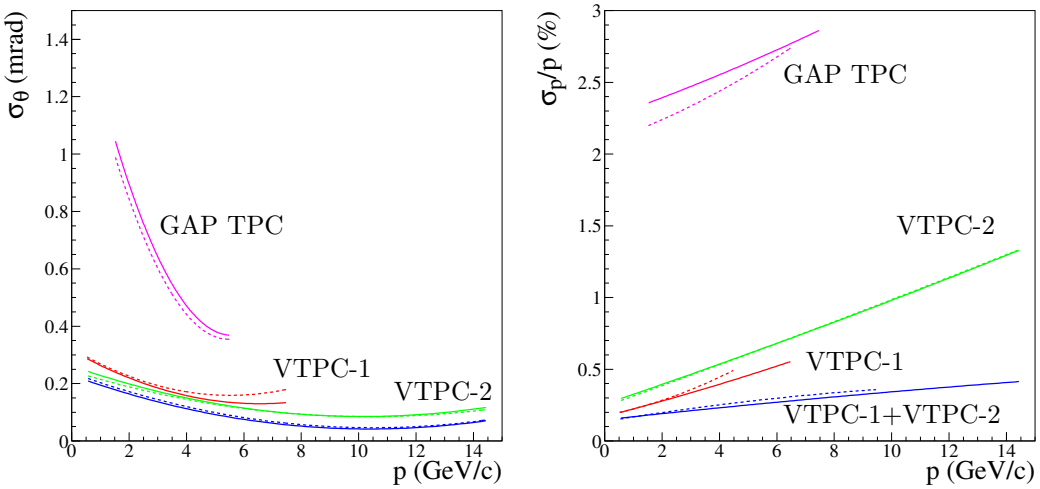

Figure 12: Error on the polar angle [left] and momentum resolution [right] as a function of momentum of the TPC tracks for data (solid) and MC (dashed). Labels refer to track topologies defined in the text.

set, the target is well aligned along the direction of the beam (no tilt), but slightly shifted by 0.2 (0.1) cm in the vertical (horizontal) plane. As depicted in Fig. 14, the target transverse dimension is well reconstructed (with a precision of 0.6 cm) using the backward extrapolation procedure, which takes into account the transverse shifts and tilt of the target in the 2007 alignment configuration. Tracks are attached along the target with a precision of 5 cm. The longitudinal position of the target is however constrained to better than 1 cm by the geometrical survey and alignment procedure.

In order to measure yields of outgoing particles in a configuration as close as possible to that of T2K (i.e. with the target aligned along the beam axis), beam tracks were selected to hit the target over the overlap region of the upstream and downstream faces, thus retaining only beam protons that effectively pass through the full length of the target (see Fig. 13). The effect of the target tilt on the yields of outgoing particles was studied over the analysis binning with dedicated MC simulations, and finally treated as an additional systematic uncertainty.

The beam and target configurations in T2K and NA61 differ also by the beam profile on target. During the 2007 data-taking period with the replica

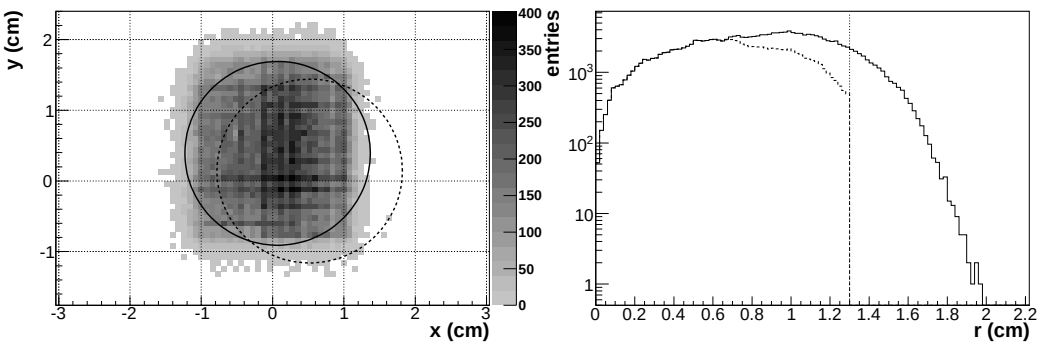

Figure 13: Profile [left] and radial distribution [right] of the beam on the upstream face of the replica target. The radial distribution is shown before (solid) and after (dashed) applying a beam track selection defined in the text. The solid (dashed) circle shows the position of the upstream (downstream) face. The dotted vertical line shows the radius of the target.

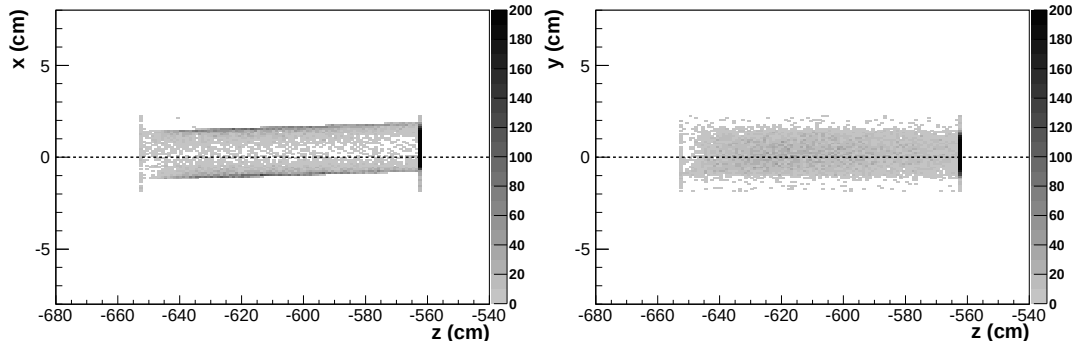

Figure 14: Distribution of the point of closest approach of the TPC tracks in the $x-z$ [left] and $y-z$ [right] projections after backward extrapolation to the surface of the target. The fact that the side of the target appears fuzzy in the vertical projection (y) is a consequence of the azimuthal acceptance of the detector (see Fig. 8) which is further constrained by the ± 30 degree wedge cut defined in the text.

target the beam was almost uniformly distributed on the target upstream face, while in T2K a narrow beam ($\sigma_{x,y} \approx$4.2 mm) well-centered on the target is used. This difference could be taken into account by re-weighting the NA61 results with the T2K beam profile in the T2K beam MC. Due to the low statistics of the 2007 data such a re-weighting was not implemented. Dedicated MC studies (reported in Section 6.2) were performed to estimate the corresponding systematic uncertainty. However, re-weighting will be applied in the analysis of the 2009 and 2010 data. For that purpose, the trigger hardware and software were upgraded before the 2009 data taking. In particular, a multi-trigger acquisition system was introduced allowing pre-scaling of different trigger types. A certain fraction of the events were recorded in a configuration that defines a beam with uniform coverage of the upstream face of the target, and in a configuration that defines a narrow, centered beam.

3.5. Particle identification

The particle identification (PID) in NA61 relies on energy loss measurements, dE/dx, in the TPCs and the time-of-flight that is used to compute the particle mass squared, m^2. For each TPC track, the dE/dx is calculated by ordering the reconstructed clusters by increasing charge and averaging the distribution over the lower 50 %. For the calculation of the mass squared, the momentum is taken without vertex constraint and the path length of the track is calculated from a plane located at the center of the target along the beam axis to the ToF-F detector. The dE/dx and mass squared distributions of the data are shown for all tracks in Fig. 15 (top panel) as a function of the track momentum.

The dE/dx can provide an efficient PID below 1 GeV/c momentum and along the relativistic rise region, but is limited in the momentum region between 1 and 3 GeV/c where the different Bethe-Bloch curves overlap. The time-of-flight provides a good discrimination between pions and protons up to 6 GeV/c. The analysis of the NA61 data with the T2K replica target is based on the combined PID method developed for the thin-target data analysis [17]. Actually, the combination of the dE/dx and time of flight provides a powerful PID over a wide momentum range. The method is illustrated in Fig. 15 (bottom panel) which depicts how the different particles (p, K, π and e) can be separated in the $(m^2, dE/dx)$ plane.

A $(m^2, dE/dx)$ distribution for positively charged tracks is obtained for each bin in (p, θ, z) determined at the surface of the replica target. The data distributions are then fit to joint probability density functions (pdf) for the

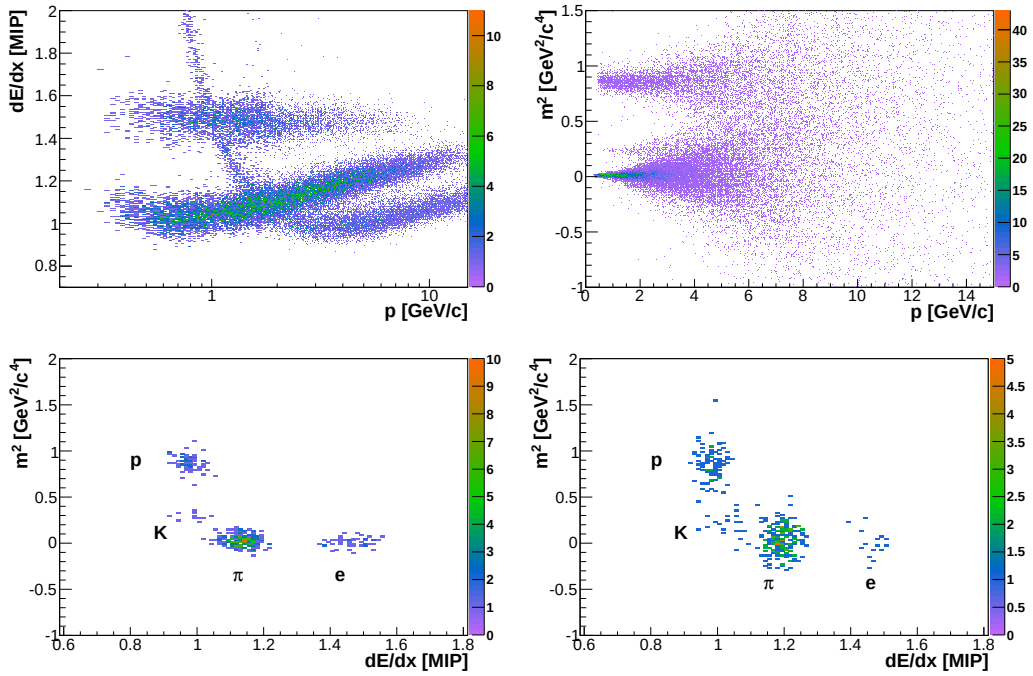

Figure 15: Top panel: dE/dx [left] and mass squared [right] distributions for all TPC tracks as a function of the track momentum at the first fitted TPC cluster. Bottom panel: $(m^2, dE/dx)$ distributions of positively charged tracks for $40 < \theta < 100$ mrad polar angle and $2.4 < p < 3.2$ GeV/c [left], $4 < p < 4.8$ GeV/c [right] momentum at the surface of the target.

mass squared and the energy loss. Due to the independence of the dE/dx and m^2 variables, the joint pdf reduces to the product of the corresponding marginal distributions which are described by Gaussian distributions. The complete pdf is a sum of two-dimensional Gaussian distributions over four particle species, p, K, π and e. For the initialisation of the fit, the resolution on the mass squared and the expected energy loss for each particle species are obtained from parametrizations of the data distributions shown in Fig. 15 as a function of the track momentum. The resolution on the expected energy loss is a function of the number of reconstructed clusters on a track ($\sim 1/\sqrt{N}$). For the topology dependent cuts defined in this analysis, it is approximated by a constant value of 3 % due to the sufficiently large number of clusters on each track. Independent normalisation factors are introduced for each particle species. Since the individual pdfs are normalised to unity, particle

yields are given by the normalisation factors which are obtained from a two-dimensional log-likelihood minimisation illustrated in Fig. 16.

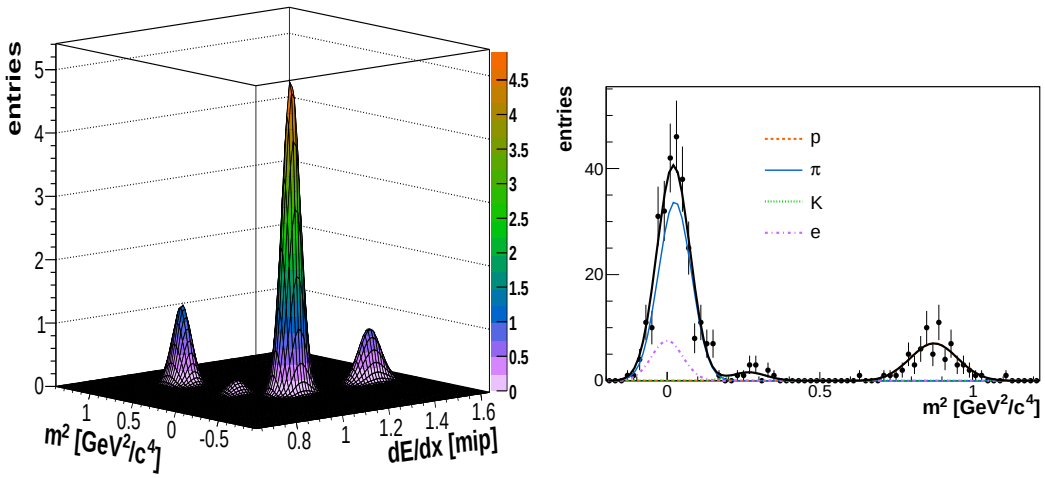

Figure 16: Two-dimensional fit of the data in the $(m^2, dE/dx)$ plane [left] and respective mass squared projection [right], for $40 < \theta < 100$ mrad and $2.4 < p < 3.2$ GeV/c at the surface of the target. The different components of the fit are shown with different line styles.

The two-dimensional fitting procedure is applied over the full momentum range of the analysis, although at high momenta when the width of the mass squared distribution becomes too large, the time-of-flight information can no longer constrain the fit significantly.

Due to the low statistics of the 2007 data, a more sophisticated pdf than a sum of two-dimensional Gaussian distributions was not justified in this analysis. For example, using multi-Gaussian distributions (i.e. a first Gaussian to describe the peak and a second one with a larger width for the tails) did not improve the results in terms of goodness of fit. It should also be noted that fits are performed in two dimensions which significantly relaxes the requirements on the pdf used to describe the data. Actually, although the one-dimensional Gaussian pdf's used for the dE/dx and m^2 might not describe tails (contaminations) of the distributions exactly, the fact that particles are well separated in two dimensions does not require a precise description of the tails in the two-dimensional case.

4. The NA61/SHINE simulation chain

In NA61 interactions of the incident proton beam inside the replica target are generated, as in the T2K beam simulation, with the FLUKA transport code: the FLUKA2011.2 version was used for this analysis since the validity period for the FLUKA2008.3d version has already expired. The FLUKA2011 version reveals a much better agreement with the published NA61/SHINE charged pion data [17] compared to the older FLUKA2008 version. Thus, no additional re-weighting of secondary $\pi^{\pm}$ is needed when FLUKA2011 version is used for neutrino flux predictions in T2K. The beam input to the standalone FLUKA simulation is based on data distributions of the beam divergence as a function of the position measured in the beam detectors located upstream of the target. The trajectory of each simulated beam track thus takes into account correlations between the position and angle of the beam protons. Particles exiting the target are stored and passed on as input to the NA61 MC detector simulation chain starting at the surface of the target. The GEANT3 [26] package then propagates particles through the magnetic field and geometry of the detectors, and simulates physics processes such as particle decays. Interactions of the tracked particles in the detector material are simulated by the GCALOR [27] model which is also used for the same purpose in the T2K beam simulation. The simulated events are processed with the same reconstruction chain as used for the real data processing.

Figure 17 shows that the employed model in the NA61 MC reasonably reproduces the kinematics of the tracks at the surface of the target for all the different topologies considered in this analysis. This is important to assure that the quality of the reconstruction of the track parameters is similar for data and MC. Actually, the latter strongly depends on the number of clusters on the track determined by the original kinematics at the surface of the target. As shown in Fig. 12, good agreement is obtained in terms of the resolution on the track parameters.

As a consequence, realistic dE/dx and m^2 values are generated for the reconstructed MC tracks by using parametrizations of the data for the mean energy loss distribution and width of the m^2 distribution as a function of the track momentum (see [31] for details).

The backward extrapolation procedure shows similar performance for MC and real data. An additional analysis was performed to extract yields of outgoing negatively charged pions in the data and the simulation. As can be seen in Fig. 18, good agreement is obtained between MC and data for the

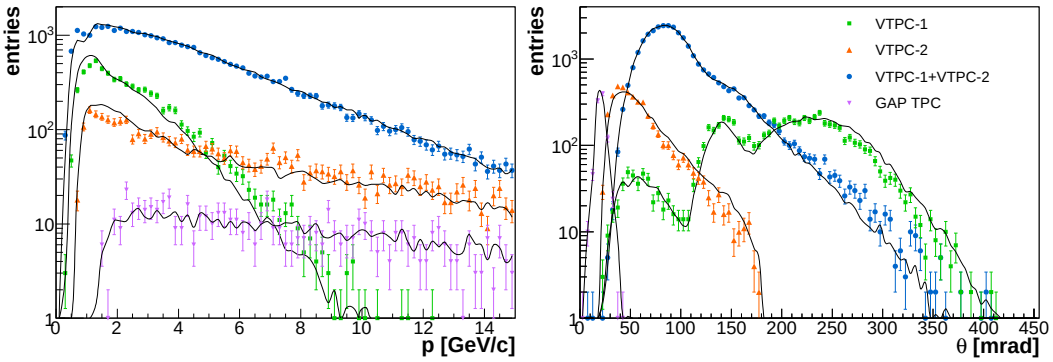

Figure 17: Distributions of momentum [left] and polar angle [right] of TPC tracks at the surface of the target for data (markers) and MC (solid smoothed curves). The different track topologies are specified in the legend on the right plot and described in the text. Small data–MC differences at large angles (above ∼250 mrad) do not influence the results reported here.

momentum distribution of negatively charged pion-like tracks after backward extrapolation, requirement of a point of closest approach closer than 0.6 cm to the surface of the target and a simple dE/dx-based PID selection to reject electrons. In both analyses, the efficiency of the procedure was estimated to be at least 98 % as a function of p, θ and z at the surface of the target.

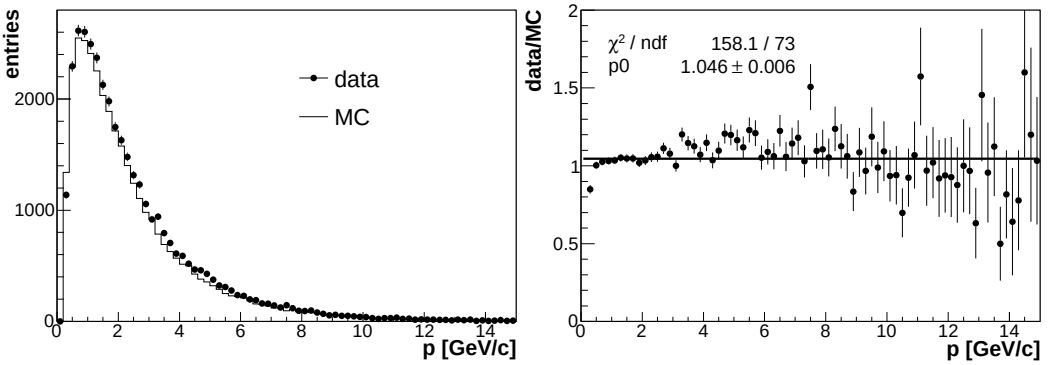

Figure 18: Momentum distribution of negatively charged pion-like tracks [left] after backward extrapolation, requirement for a point of closest approach closer than 0.6 cm to the surface of the target and a simple dE/dx-based PID selection to reject electrons. Ratio of data to MC [right].

The PID analysis applied to data described in the previous section is performed identically on the MC. Figure 19 shows the result of the log-likelihood fit to the simulated $(m^2, dE/dx)$ distribution in the (p, θ) bin shown for data in Fig. 16.

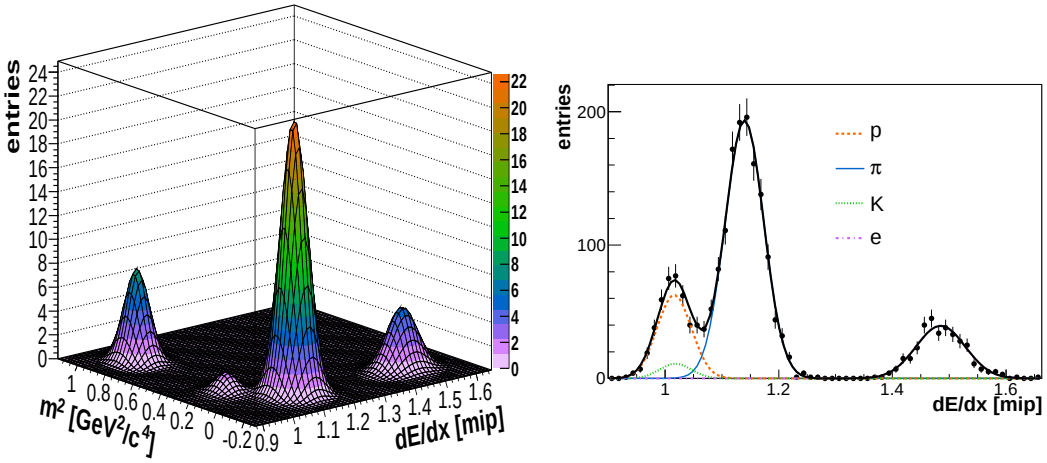

Figure 19: Two-dimensional fit of the simulated data in the $(m^2, dE/dx)$ plane [left] and respective dE/dx projection [right], for $40 < \theta < 100$ mrad and $2.4 < p < 3.2$ GeV/c at the surface of the target. The different components of the fit are shown with different line styles.

5. Yields of positively charged pions at the surface of the replica target

Yields of positively charged pions were extracted in bins of (p, θ, z) at the surface of the target for real and simulated data, using a log-likelihood fit (see Section 3.5) in the $(m^2, dE/dx)$ plane. Spectra are presented differentially as a function of momentum for different angular intervals, and different longitudinal bins along the target. For simplicity, the notations dn_{NA61}/dp and dn_{FLUKA}/dp are used to refer to the data and simulated momentum spectra respectively, in a given angular interval and longitudinal bin.

For data, the differential corrected spectra are defined as:

$$\frac{dn_{\mathrm{NA61}}}{dp} = \frac{N_{\mathrm{NA61}}}{\Delta p} \frac{1}{N^{pot}_{\mathrm{NA61}}} \prod_i \frac{1}{C^i(p, \theta, z)} \ , \qquad (1)$$

where N_{NA61} is the measured *raw* yield (i.e. after reconstruction and PID analysis) in a given angular interval and longitudinal bin for a momentum bin of width Δp, N^{pot}_{NA61} is the number of protons on target selected for the analysis, and the C^i's are correction factors that depend on the track parameters (p, θ, z). It was checked that track migration between bins is well below 10 % and thus the unfolding of the measured spectra is not necessary.

Similarly, the differential spectra obtained for FLUKA with the same PID analysis are defined as:

$$\frac{dn_{\mathrm{FLUKA}}}{dp} = \frac{N_{\mathrm{MC}}}{\Delta p} \frac{1}{N^{pot}_{\mathrm{MC}}} \prod_i \frac{1}{C^i(p, \theta, z)} \ , \tag{2}$$

where N_{MC} is the simulated *raw* yield in a given angular interval and longitudinal bin for a momentum bin of width Δp, and N^{pot}_{MC} is the number of protons on target generated for the simulation. The N_{MC} raw yield contains part of the original FLUKA information which is reconstructed within the acceptance of the detector, as well as contaminations from weak decays generated in GEANT3 and interactions in the detector material generated by the GCALOR model. Within the errors of the correction factors, dn_{FLUKA}/dp is equivalent to the original information generated at the surface of the target in the standalone FLUKA simulation.

The C^i factors in Eqs. 1 and 2 include efficiencies for the reconstruction, the backward extrapolation and the time-of-flight detector, as well as corrections for the detector geometrical acceptance, pion losses (decays and interactions in the detector material) and contamination from weak decays (feed-down). With the exception of the time-of-flight efficiency evaluated from the data, all the C^i factors are MC based corrections. These are applied identically to data and simulation and cancel in the ratio of the data and simulated yields evaluated according to Eqs. 1 and 2.

As will be further explained in Section 6.1, the use of the NA61 2007 replica-target data in T2K is based on the ratio of data and simulated yields. Thus, only *raw* yields are considered in what follows. The *raw* spectra of positively charged pions are defined following Eqs. 1 and 2 as:

$$\frac{dN_{\mathrm{NA61}}}{dp} = \frac{N_{\mathrm{NA61}}}{\Delta p} \frac{1}{N^{pot}_{\mathrm{NA61}}} \frac{1}{\epsilon^{ToF}_{\mathrm{NA61}}} \tag{3}$$

for the data, and:

$$\frac{dN_{\mathrm{MC}}}{dp} = \frac{N_{\mathrm{MC}}}{\Delta p}\frac{1}{N_{\mathrm{MC}}^{pot}} \tag{4}$$

for the MC. For data, the ToF-F detector efficiency, $\epsilon_{\mathrm{NA61}}^{ToF}$, is evaluated as a function of p and θ. Due to the ToF response not being simulated in the NA61 MC, $\epsilon_{\mathrm{MC}}^{ToF}$ is set to 1. Thus the time-of-flight detector efficiency is the only correction that does not cancel in the ratio of real data to simulation and consequently it is included in the definition of the *raw* spectra for data. As an example, *raw* spectra measured over the most upstream, central and most downstream longitudinal bins, as well as the spectra measured at the downstream face of the target are depicted in Fig. 20 in the angular interval [40-100] mrad for the real and simulated data.

Systematic uncertainties on the spectra computed via Eqs. 3 and 4 arise from the PID and normalisation for both real data and simulation. A systematic uncertainty due to the time-of-flight detector efficiency is accounted for in the data. The systematic uncertainty associated with the PID procedure was evaluated with the MC by comparing the pion yields obtained from the log-likelihood fit to the generated number of pions in the sample as a function of the reconstructed track momentum. The full statistics of the MC sample was used to estimate the uncertainty in the simulation. For the data, an independent MC sample with statistics equivalent to that of data was used. The estimated systematic uncertainty varies from 1 to 3 % for the MC and 1 to 5 % for the data with increasing momentum. A systematic uncertainty of 1.4 % was assigned to the normalisation to the number of protons on target in data. It was estimated by varying the cuts used for the selection of the beam tracks on target. The same uncertainty is propagated to the MC since the simulation of the beam tracks impinging on the target is based on real data distributions for the beam position and divergence. The systematic uncertainty associated with the ToF-F efficiency comes from the eventual inclusion of off-time tracks in the calculation. In order to estimate this uncertainty a first calculation was made using the full 50 μs drift of the MTPCs. Additional calculations were performed over only the first and last 25 μs drift distances. By comparing these calculations the uncertainty on the time-of-flight efficiency was estimated below 1 to 3 %.

The total systematic uncertainties are typically 3 to 5 % and contributions are summarized in Table 1. For data however, the overall uncertainty is dominated by the statistical uncertainty which is in the range of 10-15 %.

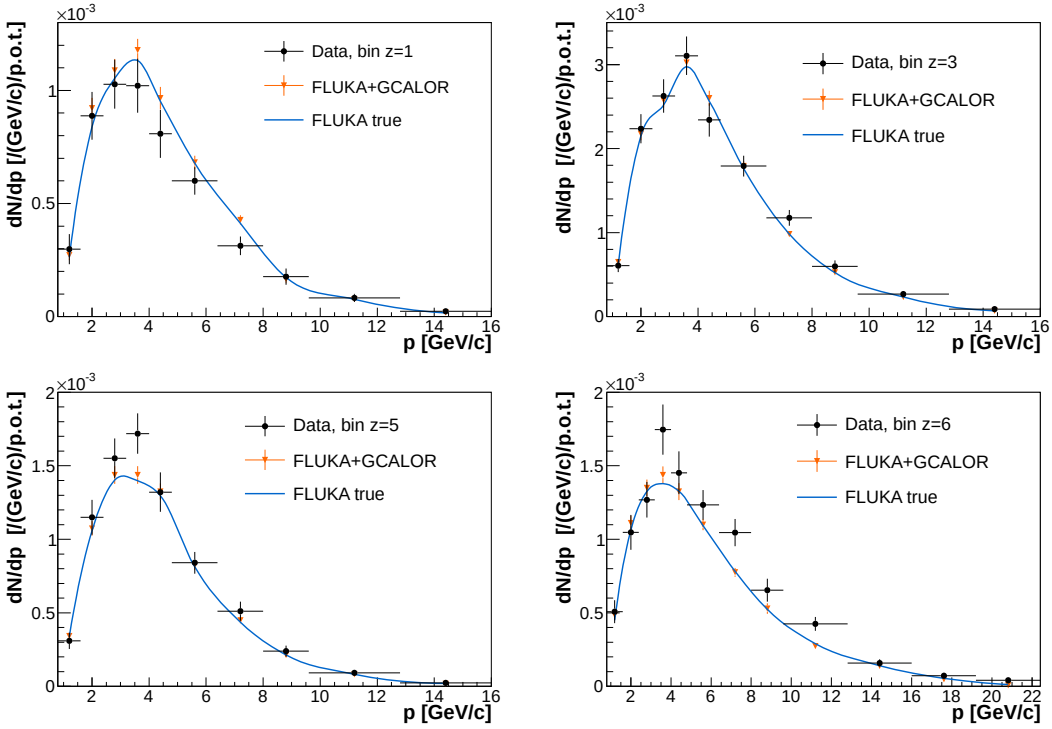

Figure 20: Spectra of outgoing positively charged pions normalised to the momentum bin size and number of protons on target in the angular interval [40-100] mrad for the most upstream [top left], central [top right] and most downstream [bottom left] longitudinal bins, and in the angular interval [0-40] mrad for the downstream face of the target [bottom right]. Error bars correspond to the sum in quadrature of statistical and systematic uncertainties. Smooth curves show the prediction of FLUKA2011.2 associated to tracks reconstructed within the acceptance of the NA61 detector (described in Section 3.4). FLUKA+GCALOR refers to the MC yields after reconstruction and PID analysis.

Table 1: Main systematic uncertainties and their dependence on momentum, p, and polar angle, θ.

systematic error	dependence	estimation	value
particle identification	p	MC	1-5%
normalization	uniform	data	1.4%
ToF efficiency	(p, θ)	data	$< 3\%$
beam momentum	uniform	MC	$< 3\%$
target density	uniform	MC	$< 3\%$
target alignment	uniform	MC	3%

6. Re-weighting of flux predictions with long-target data

6.1. Re-weighting methods

At least two different approaches based on the NA61 replica-target data can be followed to re-weight the predictions of the model used in the T2K beam MC for the simulation of hadronic interactions in the target:

1. re-weighting factors are calculated in bins of (p, θ, z) within the T2K simulation. In this case weights are defined as:

$$w(p, \theta, z) = N^{corr}_{\mathrm{NA61}}(p, \theta, z)/N^{sim}_{\mathrm{T2K}}(p, \theta, z) \ , \tag{5}$$

   where N^{corr}_{NA61} are the NA61 measured yields at the surface of the target corrected for various efficiencies, detector geometrical acceptance and particle losses (i.e. *absolute* yields), and N^{sim}_{T2K} are the yields of emitted particles *simulated* within the T2K beam MC;
2. re-weighting factors are calculated in bins of (p, θ, z) within the NA61 simulation. In this case weights are defined as:

$$w(p, \theta, z) = N^{data}_{\mathrm{NA61}}(p, \theta, z)/N^{MC}_{\mathrm{NA61}}(p, \theta, z) \ , \tag{6}$$

   where N^{data}_{NA61} are the NA61 measured yields at the surface of the target without any corrections (i.e. *raw* yields), and N^{MC}_{NA61} are the reconstructed yields obtained from the NA61 simulation based on the model used in T2K.

In the first approach, absolute yields are obtained by applying various corrections to the measured *raw* yields. This approach has the advantage that the corresponding re-weighting factors are almost model independent.

Actually, dependencies on the model used in the NA61 MC occur only via several relatively small correction factors. This includes in particular losses due to secondary interactions in the detector material or contamination from weak decays that result in a maximum 5 % correction in the NA61 2007 thin-target analysis for positively charged pions [17]. This approach does not necessarily require the use of the same hadroproduction model within NA61 and T2K.

In the second approach, which was chosen for the analysis presented in this paper, there are two prerequisites: the same MC model must be used in the T2K simulation and the NA61 analysis, and the simulated data in NA61 must go through the same reconstruction and PID analysis procedure as the real data. In this case, re-weighting factors can be calculated from *raw* yields in both data and MC since all common corrections used to obtain absolute yields in the first method will cancel in the ratio. Thus we avoid introducing additional systematic errors on top of the large statistical uncertainties of the low-statistics 2007 data. However the re-weighting factors obtained in this way are specific to the common version of the model used in both simulations (i.e. if the model were to be changed in the T2K simulation, a new set of re-weighting factors would have to be calculated within NA61).

Unlike thin-target based re-weighting factors which are calculated as ratios of production cross-sections, factors calculated with the replica-target data in both methods described above are based on yields of outgoing particles that depend upon the beam parameters of the NA61 measurements. Thus, a relative re-weighting of the NA61 and T2K beam distributions is necessary when beam distributions differ significantly in the two experiments. Eqs. 5 and 6 should then slightly be modified to account for that additional degree of freedom. The final NA61 results with the replica of the T2K target based on the high-statistics 2009 and 2010 data sets will be obtained by using the first approach which provides absolute particle yields per proton on target. As explained at the end of Section 3.4, the high statistics data will allow for the accounting for the relative re-weighting of the NA61 and T2K beams on target.

Note that a total systematic error of typically 7 % was estimated for pion spectra obtained from the 2007 thin-target data [17]. Some of the contributions to the total systematic uncertainty (e.g. feed-down correction) are expected to be significantly smaller for the T2K replica-target data. Thus, for absolute yields of particles measured at the surface of the target, we expect a precision of 5 % or better.

6.2. Application to the T2K beam simulation

T2K beam MC predictions (based on FLUKA2011.2) can be re-weighted with the NA61 2007 replica-target data by calculating the re-weighting factors defined in Eq. 6. Using Eqs. 3 and 4, these are given for each (p, θ, z) bin by:

$$w(p, \theta, z) = \frac{N_{\mathrm{NA61}}}{N_{\mathrm{MC}}} \frac{N^{pot}_{\mathrm{MC}}}{N^{pot}_{\mathrm{NA61}}} \frac{1}{\epsilon^{ToF}_{\mathrm{NA61}}} \ . \tag{7}$$

Figure 21 shows the re-weighting factors corresponding to the spectra depicted in Fig. 20, measured over the most upstream, central and most downstream longitudinal bins, as well as at the downstream face of the target.

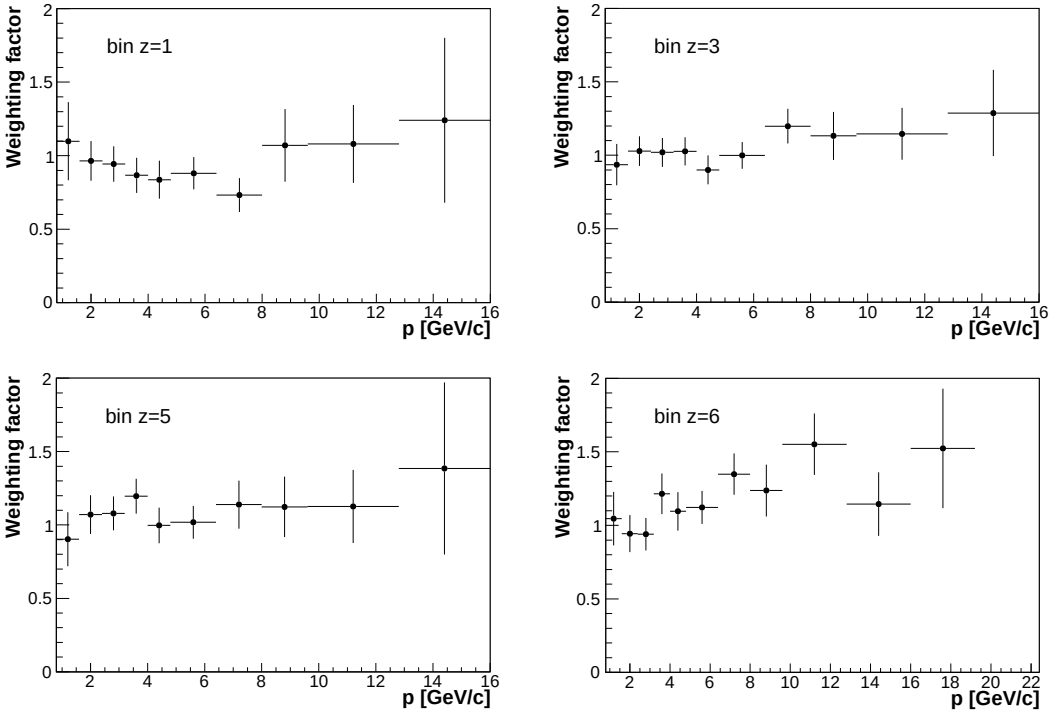

Figure 21: Re-weighting factors for outgoing positively charged pions in the angular interval [40-100] mrad for the most upstream [top left], central [top right] and most downstream [bottom left] longitudinal bins, and in the angular interval [0-40] mrad for the downstream face of the target [bottom right]. Error bars correspond to the sum in quadrature of statistical and systematic uncertainties.

In addition to the systematic uncertainties arising from the PID analysis, the normalisation and the time-of-flight detector efficiency, sources related to differences between the T2K target and the NA61 replica are accounted for in the total systematic uncertainty of the re-weighting factors. Dedicated FLUKA2011.2 simulations were performed to estimate the systematic uncertainties on the yields of outgoing charged pions due to differences in the replica-target geometry (i.e. contribution of the aluminium support flanges), alignment and density (1.83 g/cm^3 for the replica, 1.804 g/cm^3 for the T2K target) for the respective beam profiles on target in NA61 and T2K. The estimated uncertainty (within the statistical precision of the simulations) was below 3 % for the differences in target geometry and density, while an overall 3 % uncertainty was assigned for the target misalignment. An additional systematic uncertainty (< 2 %) was estimated to account for the measured width of the beam momentum distribution which is not simulated in the NA61 MC.

The overall systematic uncertainty on the re-weighting factors is typically about 6 %, with main contributions from the PID analysis at large momentum and from the target misalignment. The total error is however dominated by the statistical uncertainty which varies between 10 and 15 %.

In order to use the re-weighting factors calculated with the NA61 replica-target data in the T2K beam simulation, a new class was implemented in the existing re-weighting software based on the NA61 thin-target data (described in Ref. [28]). The class is implemented in such a way that either of two procedures can be followed to re-weight the production of positively charged pions: use of the thin-target data to re-weight the secondary and tertiary production in the target, or use of the replica-target data to re-weight outgoing pions at the surface of the target. A common re-weighting method is used for hadronic interactions that occur outside the target.

For illustration of the complete re-weighting procedure, the T2K beam simulation was run with default beam parameters in FLUKA2011.2 and horn currents set to 250 kA. The prediction of the ν_μ flux at the far detector re-weighted with the replica-target data is shown in Fig. 22 (left) together with the prediction re-weighted with the thin-target data.

For the replica-target re-weighted prediction, the maximum possible errors are shown and correspond to a fully correlated 1-sigma shift of the pion re-weighting factors only. In the case of the thin-target re-weighted prediction, two sets of errors are shown: the first one corresponds to the total error

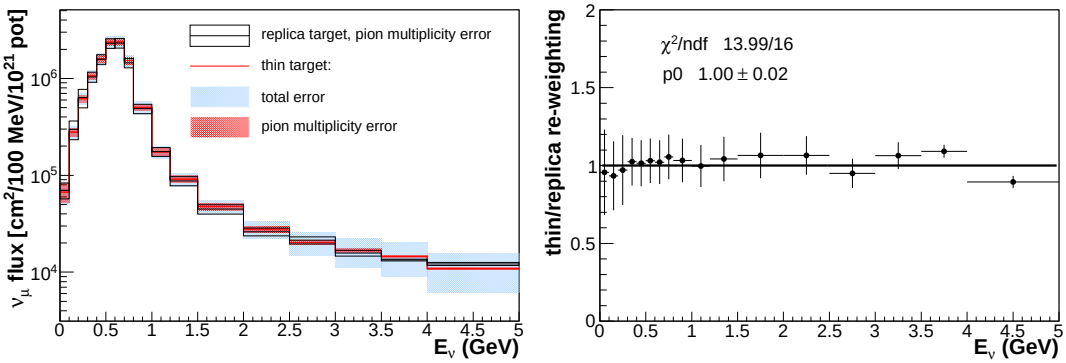

Figure 22: Re-weighted ν_μ flux predictions at the far detector of T2K based on the NA61 thin-target and replica-target data [left] and ratio of the two predictions [right]. Details about the associated errors are given in the text. A linear fit to the ratio [right] is shown by the solid line.

which is shown in fractional form in Fig. 4, the second one corresponds only to the error associated with the pion multiplicity (shown in Fig. 4 as well) and can be compared directly to the error shown for the replica-target re-weighted prediction. Large uncertainties above 2 GeV neutrino energy for the thin-target based prediction are dominated by the error propagation of the kaon re-weighting.

The ratio of the two predictions is shown in Fig. 22 (right) and indicates good agreement between the results of both methods. Errors on the ratio correspond to the error propagation in quadrature where only errors associated with the pion multiplicity are considered for the thin-target based prediction. Both re-weighting methods are consistent within the uncertainties considered in this study for the re-weighting of the pion multiplicity. Although uncertainties are of the same order for the two approaches, it should be noted that in the case of the long-target based re-weighting, results were obtained with half the statistics of the thin-target case. The analysis of the 2009 and 2010 long-target data will not only significantly decrease the dominant statistical uncertainty but also some of the currently large systematics (target misalignment).

The relative re-weighting of the NA61 and T2K beam distributions is not included at this stage of the analysis but is not expected to significantly alter the comparison presented here as a simple illustration of the re-weighting procedure.

7. Summary and conclusions

Precise predictions of the initial neutrino flux are needed by the T2K long-baseline neutrino oscillation experiment in Japan. This paper argues that the highest precision predictions can be reached by detailed measurements of hadron emission from the same target as used by T2K exposed to a proton beam of the same kinetic energy of 30 GeV. The corresponding data were recorded in 2007–2010 by the NA61/SHINE experiment at the CERN SPS using a replica of the T2K graphite target.

First, details of the experiment and data taking were described. Second, results from the pilot analysis of the NA61 data taken in 2007 with a replica of the T2K target were presented. Yields of positively charged pions were reconstructed at the surface of the replica target in bins of the laboratory momentum and polar angle as a function of the longitudinal position along the target. Third, re-weighting factors for the model used to simulate hadronic interactions in the T2K target were calculated using these measurements. As an illustration of the complete procedure, the re-weighting factors were propagated to the neutrino flux prediction in T2K. The prediction obtained in this way for the ν_μ flux at the far detector of T2K was finally compared to that obtained with a re-weighting based on the NA61 thin-target measurements.

In the global framework of accelerator-based neutrino oscillation experiments, the paper demonstrates that high quality long-target measurements can be performed with the NA61 setup and that such measurements will lead to a significant reduction of systematic uncertainties on the neutrino flux predictions in long-baseline neutrino experiments.

8. Acknowledgments

This work was supported by the Hungarian Scientific Research Fund (grants OTKA 68506 and 71989), the Polish Ministry of Science and Higher Education (grants 667/N-CERN/2010/0 and N N202 484339), the Foundation for Polish Science - MPD program, co-financed by the European Union within the European Regional Development Fund, the Federal Agency of Education of the Ministry of Education and Science of the Russian Federation (grant RNP 2.2.2.2.1547), grant 12-02-91503-CERN_a of the RFBR-CERN Foundation, the Ministry of Education, Culture, Sports, Science and Technology, Japan, Grant-in-Aid for Scientific Research (grants 18071005, 19034011, 19740162, 20740160 and 20039012), the Toshiko Yuasa Laboratory (France-Japan Particle Physics Laboratory), the Institut National de

Physique Nucléaire et Physique des Particules (IN2P3, France), the German Research Foundation (grant GA 1480/2-1), Bulgarian National Scientific Foundation (grant DDVU 02/19/ 2010), Swiss Nationalfonds Foundation (grant 200020-117913/1) and ETH Research Grant TH-01 07-3.

References

[1] Y. Itow et al. [T2K Collaboration], 2001, arXiv:hep-ex/0106019.

[2] K. Abe et al. [T2K Collaboration], The T2K Experiment. Nucl. Instrum. Meth. **A659** (2011) 106, e-Print: arXiv:1106.1238.

[3] D. Beavis et al., Long Baseline Neutrino Oscillation Experiment at the AGS (Proposal E889), 1995, Physics Design Report BNL 52459.

[4] K. Abe et al. [T2K Collaboration], Phys. Rev. Lett. **107** (2011) 041801.

[5] F. P. An et al. [DAYA-BAY Collaboration], Phys. Rev. Lett. **108** (2012) 171803.

[6] J. K. Ahn et al. [RENO Collaboration], Phys. Rev. Lett. **108** (2012) 191802.

[7] K. Abe et al. [T2K Collaboration], Phys. Rev. **D85** (2012) 031103.

[8] J. R. Sanford and C. L. Wang, "Empirical formulas for particle production in p-Be collisions between 10 and 35 BeV/c", BNL/AGS internal report JRS/CLW-1 (1967).

[9] A.J. Malensek, "Empirical Formula for Thick Target Particle Production", FERMILAB report FN-341 (1981).

[10] M. Bonesini et al., Eur. Phys. J. **C20** (2001) 13.

[11] M.G. Catanesi et al. [HARP Collaboration], Nucl. Phys. **B732** (2006) 1.

[12] M.H. Ahn et al. [K2K Collaboration], Phys. Rev. **D74** (2006) 072003.

[13] M.G. Catanesi et al. [HARP Collaboration], Eur. Phys. J. **C52** (2007) 29.

[14] A.A. Aguilar-Arevalo, FERMILAB-PUB-08-161-AD-E. Jun 2008. 74 pp., Phys. Rev. **D79** (2009) 072002, e-Print: arXiv:0806.1449.

[15] G. Ambrosini et al. [NA56/SPY Collaboration] Eur. Phys. J. **C10** (1999) 605.

[16] P. Astier et al. [NOMAD Collaboration], Nucl. Instrum. Meth. **A515** (2003) 800.

[17] N. Abgrall et al. [NA61/SHINE Collaboration], Phys. Rev. **C84** (2011) 034604.

[18] N. Abgrall et al. [NA61/SHINE Collaboration], Phys. Rev. **C85** (2012) 035210.

[19] N. Antoniou et al. [NA49-future Collaboration], Report No. CERN-SPSC-2006-034, 2006.

[20] N. Antoniou et al. [NA61/SHINE Collaboration], Report No. CERN-SPSC-2007-004, 2007.

[21] N. Antoniou et al. [NA61/SHINE Collaboration], Report No. CERN-SPSC-2007-019, 2007.

[22] N. Abgrall et al. [NA61/SHINE Collaboration], Report No. CERN-SPSC-2008-018, 2008.

[23] J. Abraham et al. [Pierre Auger Collaboration], Nucl. Instrum. Meth. A **523** (2004) 50.

[24] T. Antoni et al. [KASCADE Collaboration], Nucl. Instrum. Meth. **513** (2003) 490.

[25] A. Fasso, A. Ferrari, J. Ranft and P.R. Sala, CERN-2005-10, INFN/TC_05/11, SLAC-R-773.

[26] R. Brun, F. Bruyant, M. Maire, A.C. McPherson and P. Zanarini, GEANT3, CERN-DD-EE-84-1.

[27] `http://www.atlas.uni-wuppertal.de/zeitnitz/gcalor`

[28] V. Galymov, Contribution to NUFACT11, XIIIth International Workshop on Neutrino Factories, Super Beams and Beta Beams, 1-6 Aug. 2011, CERN and University of Geneva. Submitted to IOP conference series.

[29] S. Afanasiev et al. [NA49 Collaboration], Nucl. Instrum. Meth. A **430** (1999) 257.

[30] K. Matsuoka *et al.*, Nucl. Instrum. Meth. A **624** (2010) 591.

[31] N. Abgrall, PhD thesis, CERN-THESIS-2011-165, available on `http://weblib.cern.ch`